



Cite this: *J. Mater. Chem. C*, 2020, **8**, 5476

# Photoswitchable fluorescent polymer nanoparticles as high-security anticounterfeiting materials for authentication and optical patterning†

Amin Abdollahi, <sup>a</sup> Hossein Alidaei-Sharif,<sup>a</sup> Hossein Roghani-Mamaqani <sup>\*ab</sup> and Ata Herizchi<sup>c</sup>

Invisible high-security anticounterfeiting polymeric inks exhibiting both photochromism and fluorescence emission for security marking have attracted significant interest recently. In the current study, flexible and invisible high-security anticounterfeiting inks were developed via the chemical incorporation of spiropyran into copolymer latex nanoparticles based on methyl methacrylate and butyl acrylate by semi-continuous miniemulsion polymerization. The anticounterfeiting inks are based on latex nanoparticles with various polarities and glass transition temperatures ( $T_g$ ) and have spherical morphology with narrow size distribution in the range of 50–80 nm. The inks can simultaneously display photochromism (colorless to purple) and fluorescence emission (highly intense and bright red emission) upon UV irradiation in a fast and facile manner using a minimum concentration of spiropyran (about 1 wt% with respect to the polymer content). The morphology investigation and measurement of contact angles on the surface of the papers impregnated with stimuli-chromic latex samples display that the latex nanoparticles with different flexibilities have appropriate coating ability and stability on the surface of the cellulosic substrates due to the formation of hydrogen bonding. The investigation of the photochromic properties and fluorescence emission of the samples shows that the latex particles with higher polarity of the polymer chains have significant photochromic intensity and fluorescence emission as well as high photofatigue resistance, photoswitchability, and reversibility without displaying negative photochromism. Fast responsivity upon UV irradiation was observed for the sample with a  $T_g$  of about 33 °C and medium polarity, which indicated that the kinetics of the SP  $\leftrightarrow$  MC isomerization was a function of the polarity and flexibility of the polymer chains. The invisible high-security ink prepared using the photochromic and fluorescent latex nanoparticles with the highest optical properties was loaded on a stamp with different marks and used for print-marking different security documents, such as a certificate, money, and passport. The printed marks and finger-print on the security documents displayed photochromism and red fluorescence upon UV irradiation (365 nm). Spraying the latex nanoparticles on cellulosic papers induced high-resolution rewritable photopatterns on the cellulose substrate after UV illumination under different masks. Thus, the strategy developed to prepare high-security anticounterfeiting inks is an efficient, facile, and fast method for authentication applications.

Received 23rd February 2020,  
Accepted 9th March 2020

DOI: 10.1039/d0tc00937g

rsc.li/materials-c

<sup>a</sup> Faculty of Polymer Engineering, Sahand University of Technology, P.O. Box: 51335-1996, Tabriz, Iran<sup>b</sup> Institute of Polymeric Materials, Sahand University of Technology, P.O. Box 51335-1996, Tabriz, Iran<sup>c</sup> Faculty of Chemical Engineering, Sahand University of Technology, P.O. Box 51335-1996, Tabriz, Iran. E-mail: r.mamaghani@sut.ac.ir† Electronic supplementary information (ESI) available: <sup>1</sup>H NMR spectra of all the stimuli-chromic latex samples for the determination of DP and MW, SEM image of PMMA and fluorescence spectrum of PMMA-SP (excited at 410 nm and emission at 715 nm), further experiments for the determination of the solid content in the latex samples, a table and images of the CIE 1931 chromaticity diagram, and contact angle investigations are presented. See DOI: 10.1039/d0tc00937g

## 1. Introduction

Counterfeiting and copying security documents have resulted in considerable attention being focused on the development of anticounterfeiting and authentication technologies based on fluorescent materials such as semiconductor nanocrystals<sup>1–3</sup> and nanorods,<sup>4</sup> inorganic perovskite nanocrystals,<sup>5–7</sup> rare earth-doped nanostructures,<sup>8–10</sup> metal nanoclusters and complexes,<sup>11–13</sup> polymer nanoparticles,<sup>14–17</sup> carbon and polymer dots,<sup>18–20</sup> and quantum dots.<sup>21</sup> High-security materials are highly demanded in the anticounterfeiting ink industry. For this purpose,

light-responsive compounds with dual security marks such as fluorescence, phosphorescence, photochromism, thermochromism, mechanochromism, and hydrochromism are desirable.<sup>16,22</sup> Photochromism and fluorescence are highly significant because of their visibility (color change and fluorescence emission, respectively) upon UV light irradiation in a fast and facile manner.<sup>16,23–27</sup> However, a significant challenge in this field is the decrease in the photostability and lifetime of fluorescent compounds because of dye aggregation and the release of chromophores into the environment. These problems can be solved by using polymer nanoparticles as carriers for the encapsulation of fluorescent compounds, which can protect against environmental degradation.<sup>28–30</sup>

Stimuli-responsive polymer nanoparticles are a significant category of smart materials, which have attracted significant attention because of their potential applications in bioimaging, drug-delivery, gene delivery, cell labeling, anti-counterfeiting inks, and photopatterning.<sup>31–40</sup> Among the different smart polymers, light-responsive polymer nanoparticles are very interesting because of their unique characteristics such as fast responsivity, reversibility, photoswitchability, and photofatigue resistance.<sup>23,27,41–43</sup> In addition, light is a physical stimulus, which is controllable outside the system, tunable in intensity, non-destructive, and available at any time and place.<sup>44–48</sup> Generally, photochromic polymer nanoparticles are prepared *via* the incorporation of photochromic compounds into hydrophobic polymer matrices during copolymerization, post-polymerization modification, and doping. However, the copolymerization and post-polymerization modification strategies are more interesting than the doping method because of their advantages in increasing the photochromism lifetime, reversibility, and light-responsivity under high UV/visible irradiation cycles. Spiropyran is one of the important organic photochromic compounds extensively used in the development of stimuli-chromic polymers because of its unique photochromic behavior and fluorescence emission upon different stimuli.<sup>16,22</sup> Spiropyran displays coloration and chromism phenomena in response to different stimuli such as light, acid, solvent, ion, mechanical force, and electrical potential, which are known as photochromism,<sup>49</sup> acidochromism,<sup>50</sup> solvatochromism,<sup>42</sup> ionochromism,<sup>51</sup> mechanochromism<sup>52</sup> and electrochromism,<sup>53</sup> respectively. Therefore, spiropyran has been extensively used in development of different stimuli-chromic polymers with advanced applications in optical-chemosensors for the photosensing of different analytes, chemicals, and mechanical forces.<sup>16</sup> In addition to chemosensor applications, spiropyran is an important candidate for the development of anticounterfeiting polymer inks and photopatterning on different substrates. Spiropyran displays coloration and red fluorescence emission upon UV irradiation, which are reversed to the initial discolored and non-fluorescent structure in response to visible light, respectively. Correspondingly, the discolored, non-planar, and non-polar spiro (SP) form is converted to the colored, planar, and zwitterionic merocyanine (MC) form, where the MC form is returned to the SP form upon visible light irradiation or heating.<sup>23–27,42,54</sup> Thus, this chromophore can induce reversible coloration (photochromism) and fluorescence emission in polymers *via* its physical or

chemical incorporation into polymer matrices. The MC structure can significantly be affected by different properties of the media and polymer matrix.<sup>26,42</sup> For example, the polarity and chain flexibility of polymers can influence the kinetics of SP  $\leftrightarrow$  MC isomerization, negative or positive photochromism, photoswitchability, and reversibility (photofatigue resistance), and coloration or fluorescence emission. Therefore, the characteristics of the polymer matrix are determinative factors in the final properties of spiropyran-containing polymers, especially photochromism and fluorescence emission as two important properties required in anticounterfeiting applications. Most of the studies on spiropyran-based photochromic polymers have focused on the preparation of polymer nanoparticles by emulsion, mini-emulsion, and emulsifier-free emulsion polymerization.<sup>23,25,27,55</sup> Spiropyran can induce both photochromism and fluorescence security marks in polymeric anticounterfeiting inks, which is known as high-security materials.<sup>25,56–58</sup>

The preparation and applications of different stimuli-chromic polymer nanoparticles based on spiropyran have extensively been studied.<sup>23,26,55,59</sup> The chemical incorporation of spiropyran into different polymer matrices and chemical attachment of the resulting latex particles to different substrates significantly affect the reversibility, photoswitchability, and photofatigue resistance of the photochromism in spiropyran.<sup>27,60</sup> In anticounterfeiting inks based on spiropyran-containing stimuli-chromic latex nanoparticles,<sup>24,25</sup> the prepared stimuli-chromic latexes can directly be used for marking different security documents such as money and certificates, which display coloration after UV irradiation and red fluorescence under UV irradiation. Wang and coworkers<sup>56</sup> reported the preparation of inks with applications in anticounterfeiting quick-response codes based on metal-organic frameworks. Kalytchuk and coworkers<sup>61</sup> focused on the design of new anticounterfeiting inks based on carbon dot fluorescent materials. These smart inks are generally prepared *via* the physical incorporation of luminescent organic and inorganic compounds into a matrix, and the resulting security marks were observable only under UV irradiation as a result of fluorescence emission. However, spiropyran, is a chemically attachable photochromic and fluorescent compound on polymer particles, and has a long life. Most of the polymer inks reported to date are non-flexible since the glass transition temperature ( $T_g$ ) of the polymer matrix is above ambient temperature. This reduces the stability of the inks on paper surface and also their photochromism kinetics and fluorescence emission. Thus, the development of flexible anticounterfeiting inks based on polymer nanoparticles (below 100 nm) containing the minimum concentration of spiropyran with high photochromism and fluorescence intensity is an interesting challenge, which is the aim in the current study.

Herein, flexible anticounterfeiting inks based on stimuli-chromic latex nanoparticles containing spiropyran were prepared through semi-continuous mini-emulsion polymerization. Accordingly, a series of latex samples with a broad range of  $T_g$  (–50 to 150 °C) were prepared *via* the copolymerization of methyl methacrylate (MMA), butyl acrylate (BA), and 1 wt% of spiropyran ethyl acrylate monomer (SPEA). Differential scanning

calorimetry (DSC) analysis was used to determine the  $T_g$  of the copolymer samples. The morphology, size, and size distribution of the stimuli-chromic latex nanoparticles were investigated *via* dynamic light scattering (DLS), transmission electron microscopy (TEM), and scanning electron microscopy (SEM). The photochromic properties, photoswitchability, photofatigue resistance, reversibility, kinetics of the SP  $\leftrightarrow$  MC isomerization, and chromaticity diagrams were studied *via* UV-Vis spectroscopy, in addition to the fluorescence emission investigation by fluorescence spectroscopy. Furthermore, the stimuli-chromic latex nanoparticles were used as photochromic/fluorescent anticounterfeiting inks for print-marking security documents by different stamps and fingerprints and applying photopatterns on cellulosic papers using various masks. Surface-covering of the cellulosic papers and cotton fibers with latex nanoparticles was investigated by SEM and contact angle measurements on the surface of impregnated paper and tissue in the corresponding latexes. These water-based latex samples showed a particle size in the range of 50–80 nm with a narrow distribution and also various  $T_g$  values; therefore, they have potential applications in security print-marking and photopatterning as flexible and printable polymer inks.

## 2. Experimental

### 2.1. Materials

2,3,3-Trimethylindolenin, 2-bromoethanol, and 2-hydroxy-5-nitrobenzaldehyde were purchased from Sigma-Aldrich and used for the synthesis of (*R/S*)-2-(3',3'-dimethyl-6-nitro-3'*H* spiro[chromene-2,2'-indol]-1'-yl)ethanol (SPOH). Polyethylene glycol (PEG, 3500–4500 g mol<sup>-1</sup>), glycerol, phosphotungstic acid, and hexadecane (HD) were also purchased from Sigma-Aldrich. Acryloyl chloride, methyl methacrylate (MMA), butyl acrylate (BA), azobisisobutyronitrile (AIBN), SPAN 80, sodium hydrogen carbonate (NaHCO<sub>3</sub>), sodium dodecyl sulfate (SDS), and all solvents were supplied from Merck Chemical Company. High-quality filter paper (Whatman qualitative filter paper for technical use, product number: WHA10347512, creped circles with a diameter of 185 mm, Germany), general purpose cotton tissue, and distilled-deionized (DI) water were also used. All the materials were used without further purification.

### 2.2. Synthesis of SPOH and SPEA

SPOH was prepared according to the procedure reported by Raymo and coworkers.<sup>62</sup> In addition, SPOH was modified to spiropyran ethyl acrylate (SPEA) monomer according to the literature.<sup>23</sup> The chemical structure of SPEA was characterized *via* <sup>1</sup>H NMR spectroscopy (DMSO, 400 MHz) and the obtained spectrum was reported in our previous works.<sup>24,25</sup>

### 2.3. Preparation of the fluorescent and photochromic latex nanoparticles

Stimuli-chromic latex nanoparticles with a solid content of about 10 wt% were prepared *via* mini-emulsion polymerization. In a typical procedure, a mixture of MMA, BA, NaHCO<sub>3</sub>, SDS, HD, DI water, and SPAN 80 (with the amounts presented in Table S1, ESI<sup>†</sup>) was emulsified three times (10 min) by probe

sonication at 75% amplitude. The emulsified mixture was transferred to a three-neck round-bottom flask equipped with a condenser and nitrogen gas inlet under magnetic stirring at 400 rpm. To initiate the polymerization reaction, AIBN (0.1 g) was added to the resulting milk-like mixture and the temperature was set at 80 °C. For the chemical incorporation of spiropyran into the latex nanoparticles, an aqueous solution of SPEA (0.05 g in 1 mL water) was added dropwise to the reaction mixture over 30 min, 1 h after the initiation of polymerization. After the addition of SPEA, the polymerization reaction was continued for 3 h to obtain stimuli-chromic latex nanoparticles with a monomer conversion of above 95% and also coagulation content of below 0.5% (determined by the method presented in the ESI<sup>†</sup>). The total amount of incorporated SPEA in the latex nanoparticles was determined by coagulation of the latex samples and absorption measurement of the remaining serum by UV-Vis analysis with respect to the standard solution and the corresponding calibration curve. It was found that more than 95% of the added SPEA was incorporated in the samples. The chemical structure, molecular weight (MW), and number-average degree of polymerization (DP) of the samples were investigated by <sup>1</sup>H NMR (CDCl<sub>3</sub>, 300 MHz). The corresponding spectra are displayed in Fig. S1 (ESI<sup>†</sup>) for PBA-SP, PBAMMA-SP1, PBAMMA-SP2, PBAMMA-SP3, and PMMA-SP.

### 2.4. Preparation of invisible fluorescent and photochromic anticounterfeiting inks

The invisible fluorescent and photochromic anticounterfeiting inks were prepared by mixing a solution of PEG (0.5 g, molecular weight of about 4000 g mol<sup>-1</sup>) and glycerol (0.5 g) in 4 mL ethanol with 10 mL of latex sample under ambient conditions with stirring for 24 h. PEG and glycerol were added to increase the viscosity of the inks to 1.24 cP at 25 °C, and ethanol was added to decrease the drying time after printing on paper. After completion of the required mixing time, the homogenous colloidal inks with a solid content of about 13.3 wt% could be used for hand-writing by pen and print-marking by a stamp for labeling security documents.

### 2.5. High-security anticounterfeiting print-marking and erasable photopatterning

The anticounterfeiting inks were directly charged into the designed stamps without any additives, and then applied on a certificate, money, and passport to induce high-security anticounterfeiting print-marks with both photochromism and fluorescence emission characteristics. In addition, rewritable photopatterns were prepared by spraying the initial photochromic and fluorescent latex nanoparticles on cellulosic papers and then drying at 45 °C for 5 h. These papers were exposed to UV irradiation (365 nm) under various masks for 5 min, and the photopatterns were investigated by taking photos before and after UV light illumination. Discoloration of the patterns was carried out by visible light illumination and also heating at 40 °C for 5 min.

### 2.6. Characterization

The chemical structure of SPOH and SPEA was characterized by proton nuclear magnetic resonance (<sup>1</sup>H NMR) spectroscopy

using a Bruker DPX 400 MHz apparatus in  $\text{CDCl}_3$ . Differential scanning calorimetry (DSC) was carried out under an  $\text{N}_2$  atmosphere at a heating rate of  $10\text{ }^\circ\text{C min}^{-1}$  using an NETZSCH Instruments Co. DSC 200, F3Maia, Germany in the temperature range of  $-100$  to  $150\text{ }^\circ\text{C}$ . The DSC samples were prepared by coagulation of the latex nanoparticles, washing with water and ethanol three times to remove non-polymeric additives such as surfactants, and drying in a vacuum oven at  $40\text{ }^\circ\text{C}$  for 24 h. The particle size and distribution were measured using a ZETASIZER NANO ZSP dynamic light scattering instrument (DLS, Malvern, United Kingdom) at  $25\text{ }^\circ\text{C}$ . For this, the initial latex nanoparticles were diluted with DI water to reach a concentration of about  $1\text{ mg mL}^{-1}$ . Field-emission scanning electron microscopy (FE-SEM) micrographs were recorded on a Tescan Mira III (Czech Republic). For the preparation of the samples, a drop of diluted latex sample was placed on the sample holder and dried under vacuum at  $25\text{ }^\circ\text{C}$ . Then, it was placed in a vacuum, evacuated, and a layer of gold was deposited under flushing with argon using an EMITECH K450x sputter-coater (England). Transmission electron microscopy (TEM) images were taken using a LEO 906 instrument (Zeiss, Oberkochen, Germany) with an accelerating voltage of 100 kV to study the morphology of the latex nanoparticles. For this, a drop of sample (with concentration of about  $1\text{ mg mL}^{-1}$ ) was placed on the carbon-coated copper grid and dried under vacuum at  $25\text{ }^\circ\text{C}$ . The photochromic properties of the samples were investigated *via* UV-Vis analysis by using an EU2200 UV-Vis ONLAB Instruments (China). The fluorescence emission of the samples was investigated using a JASCO FP-750 spectrofluorometer (Japan). Diluted latex nanoparticle samples with a concentration of  $1\text{ mg mL}^{-1}$  were used for the UV-Vis and fluorescence spectroscopy analysis. To evaluate the photochromic properties, excitation was performed using a UV lamp ( $365\text{ nm}$ ,  $6\text{ W m}^{-2}$ ), CAMAG 12VDC/VAC ( $50/60\text{ Hz}$ ,

14VA, Switzerland). Also, the visible light source was a common LED lamp ( $8\text{ W m}^{-2}$ ). The UV and visible irradiation times were set at 5 min for all samples. The contact angle of a water droplet on the surface of impregnated papers with the stimuli-chromic latex samples was measured using a KRUSS G10 (Germany) at room temperature and 25% relative humidity. The CIE position color analysis was conducted by measuring the transmittance according to ASTM E1348 and ASTM D2244 by using a Gretag Macbeth CE7000 A spectrophotometer.

### 3. Results and discussion

Spiropyran is highly interesting for the development of high-security anticounterfeiting inks because of its photochromism and fluorescence emission in response to UV light. In the current study, stimuli-chromic latex nanoparticles containing spiropyran were synthesized by mini-emulsion polymerization, and used in development of anticounterfeiting inks with applications in high-security print-marking and photopatterning on cellulosic substrates. As schematically shown in Fig. 1, stimuli-chromic latex nanoparticles with different  $T_g$  values were prepared by semi-continuous mini-emulsion copolymerization of MMA and BA in the presence of SPEA as the photochromic comonomer according to the procedure presented in Table S1 (ESI<sup>†</sup>). The dropwise addition of SPEA solution after 1 h from the beginning of the polymerization reaction resulted in the incorporation of spiropyran molecules in the surface and outer layers of the latex nanoparticles. The final application of these latex samples is related to their photochromism and fluorescence emission characteristics under UV irradiation, which are affected by the concentration of spiropyran at the particle surface absorbing UV irradiation and displaying coloration

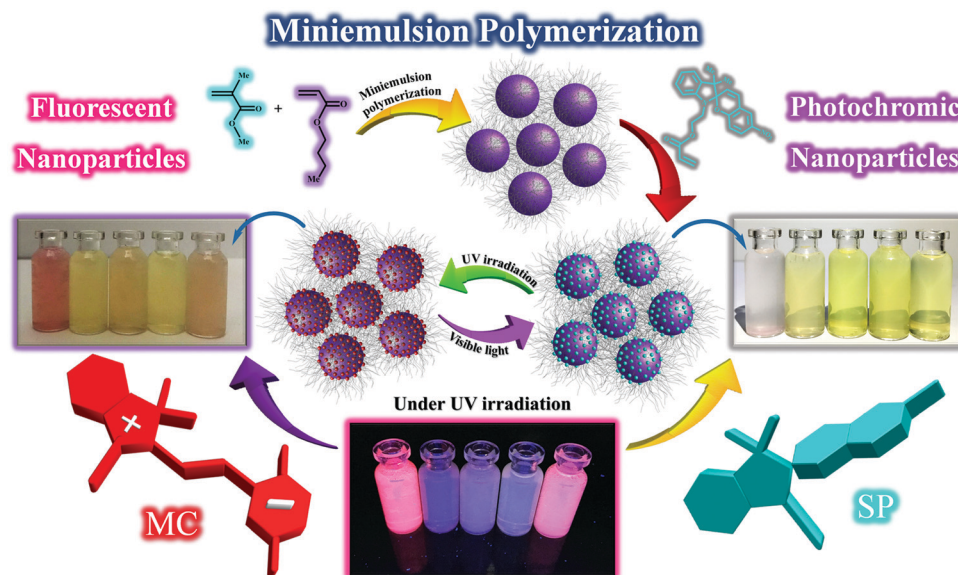


Fig. 1 Schematic illustration of the preparation of the stimuli-chromic latex nanoparticles with different  $T_g$  values by semi-continuous mini-emulsion polymerization, and photochromism and fluorescence emission of the stimuli-chromic latex nanoparticles (with a solid content of about 0.1 wt%) under UV and visible light irradiation. The samples are PMMA-SP, PBA-SP, PBAMMA-SP1, PBAMMA-SP2, and PBAMMA-SP3 from the left to right, respectively.

and red fluorescence. This is an important reason for the incorporation of spiropyran molecules on the surface of the latex nanoparticles, which was carried out by feeding SPEA in the reaction mixture after polymerization was initiated. To confirm the chemical structures of the copolymer samples and also determine their molecular weight (MW) and number-average degree of polymerization (DP), all the copolymer samples were analyzed by  $^1\text{H}$  NMR, as shown in Fig. S1 (ESI $^\dagger$ ) for PBA-SP, PBAMMA-SP1, PBAMMA-SP2, PBAMMA-SP3, and PMMA-SP. The DP values of these samples are very close to the monomer feed ratio presented in Table S1 (ESI $^\dagger$ ), which confirms the efficiency of the copolymerization method for the preparation of random copolymers of BA and MMA. A lower concentration of spiropyran in the copolymer samples resulted in its absence in the  $^1\text{H}$  NMR spectra. As shown in Fig. 1, the prepared latex samples displayed coloration in response to UV irradiation, resulting from the isomerization of the colorless SP to the colored MC form. In addition, latex nanoparticles with  $T_g$  in the range of  $-60$  to  $110$   $^\circ\text{C}$  were synthesized by homopolymerization and copolymerization of MMA and BA in different ratios. The aim was to investigate the effect of chain flexibility and polarity of the latex nanoparticles on the photochromism and fluorescence emission of spiropyran upon UV irradiation. MMA and BA are polar and non-polar monomers with polymers showing high and low  $T_g$  values, respectively. Consequently, different ratios of MMA and BA in the latex samples can significantly influence the stimuli-chromic characteristics.

### 3.1. Determination of chain flexibility for the stimuli-chromic latex samples

The latex samples containing different contents of BA and MMA have different  $T_g$  and chain flexibility, which affect the photochromism and fluorescence emission of the spiropyran molecules. The SP  $\leftrightarrow$  MC isomerization upon UV and visible light irradiation requires chain flexibility of the host matrix and free volume for molecular motion from the non-conjugated and non-planar SP form to the conjugated and planar MC structure. A decrease of  $T_g$  can result in an increase in chain mobility and free volume and acceleration of the isomerization reaction.

Therefore, stimuli-chromic latex nanoparticles with different  $T_g$  values were synthesized to investigate the relation between the photochromic properties and fluorescence emission with chain flexibility. For the determination of the  $T_g$  values by DSC analysis, the latex samples were coagulated and washed with water and ethanol three times to remove non-polymeric additives such as surfactants, and then dried in a vacuum oven at  $40$   $^\circ\text{C}$  for 24 h. Fig. 2(A) displays the DSC thermograms for poly(methyl methacrylate) (PMMA), poly(butyl acrylate) (PBA), and the different copolymers of BA and MMA. The PBA and PMMA samples showed a transition at about  $-48.1$  and  $111.2$   $^\circ\text{C}$ , which indicates the flexible and brittle nature of the PBA and PMMA samples, respectively. The PBAMMA sample displayed a single transition at about  $13.7$   $^\circ\text{C}$ , which confirms the successful copolymerization reaction. Fig. 2(B) displays the DSC thermograms obtained for the stimuli-chromic copolymer samples containing spiropyran pendant groups. The amount of spiropyran chromophore was constant for all the samples (1 wt% with respect to the total monomer), and the ratio of BA and MMA was different in the stimuli-chromic latex samples. The single transition for all the samples confirms the efficiency of copolymerization reaction of BA, MMA, and SPEA. The results display that the  $T_g$  of the samples dramatically increased with a decrease in BA content, where the stimuli-chromic latex samples have a wide range of  $T_g$  values from  $-50$  to  $112$   $^\circ\text{C}$ . The  $T_g$  values obtained from the DSC thermograms for all the samples are close to the theoretical values calculated from the Flory–Fox equation. The negligible difference between the experimental and theoretical  $T_g$  values is due to the effect of the spiropyran pendant groups. According to the DSC results, stimuli-chromic latex nanoparticles with different chain flexibility were successfully synthesized, where the spiropyran molecules were chemically incorporated as pendant groups in the polymer chains.

### 3.2. Investigation of the size and morphology for the stimuli-chromic latex nanoparticles

The particle size and distribution for the stimuli-chromic latex nanoparticles were studied by DLS analysis and the results are

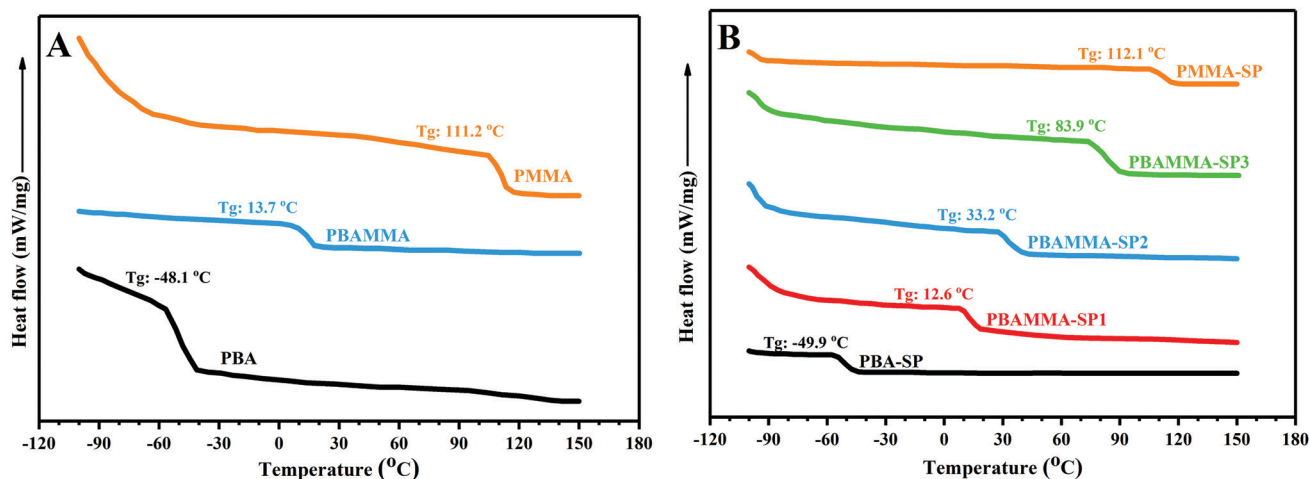


Fig. 2 DSC thermograms for the latex samples: (A) without spiropyran and (B) containing 1 wt% of spiropyran chromophore.

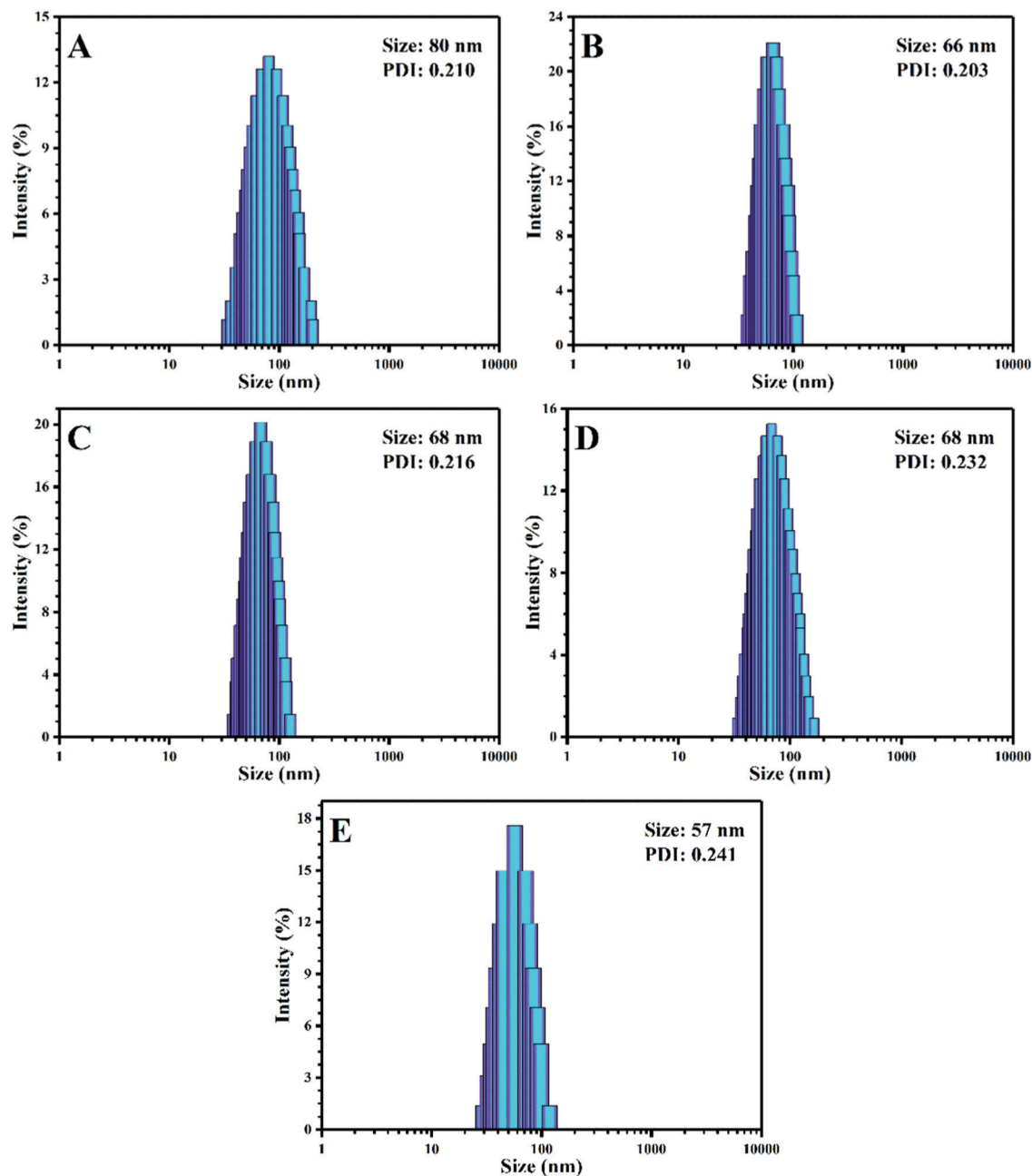


Fig. 3 DLS results for the stimuli-chromic latex nanoparticles: (A) PBA-SP, (B) PBAMMA-SP1, (C) PBAMMA-SP2, (D) PBAMMA-SP3, and (E) PMMA-SP.

presented in Fig. 3. The latex samples are expected to have a particle size below 100 nm with a narrow distribution because of their preparation method of semi-continuous mini-emulsion polymerization, which is an efficient strategy for the preparation of nanoparticles. The addition of SPEA after initiation of the polymerization reaction may induce secondary nucleation in the system. However, the polydispersity index (PDI) in the range of 0.2–0.24 shows that the spiropyran molecules were incorporated into the latex nanoparticles without any secondary nucleation (Fig. 3). The latex nanoparticles show a size in the range of 50–80 nm, which is close to that of the PBA-SP and PMMA-SP samples (80 and 57 nm, respectively). The final latex samples did not show coagulation of more than 0.5 wt%. In addition,

their colloidal stability was very high, and coagulation was not observed even 4 months after their synthesis.

For the morphological investigation of the latex nanoparticles by SEM analysis, 9 mL of the latex samples with a concentration of  $1 \text{ mg mL}^{-1}$  was mixed with 1 mL of phosphotungstic acid solution (aqueous solution, 1 wt%). Phosphotungstic acid was used to inhibit the deformation of the nanoparticles upon exposure to the SEM beams because of their low  $T_g$  and small size. As shown in Fig. 4(A and B), the PBA-SP latex nanoparticles were deformed and coagulated upon exposure to the SEM beams and increase in temperature, which is because of their high-flexibility and low  $T_g$  value. The SEM image of PBAMMA-SP1 in Fig. 4(C) displays spherical nanoparticles with a diameter of less than

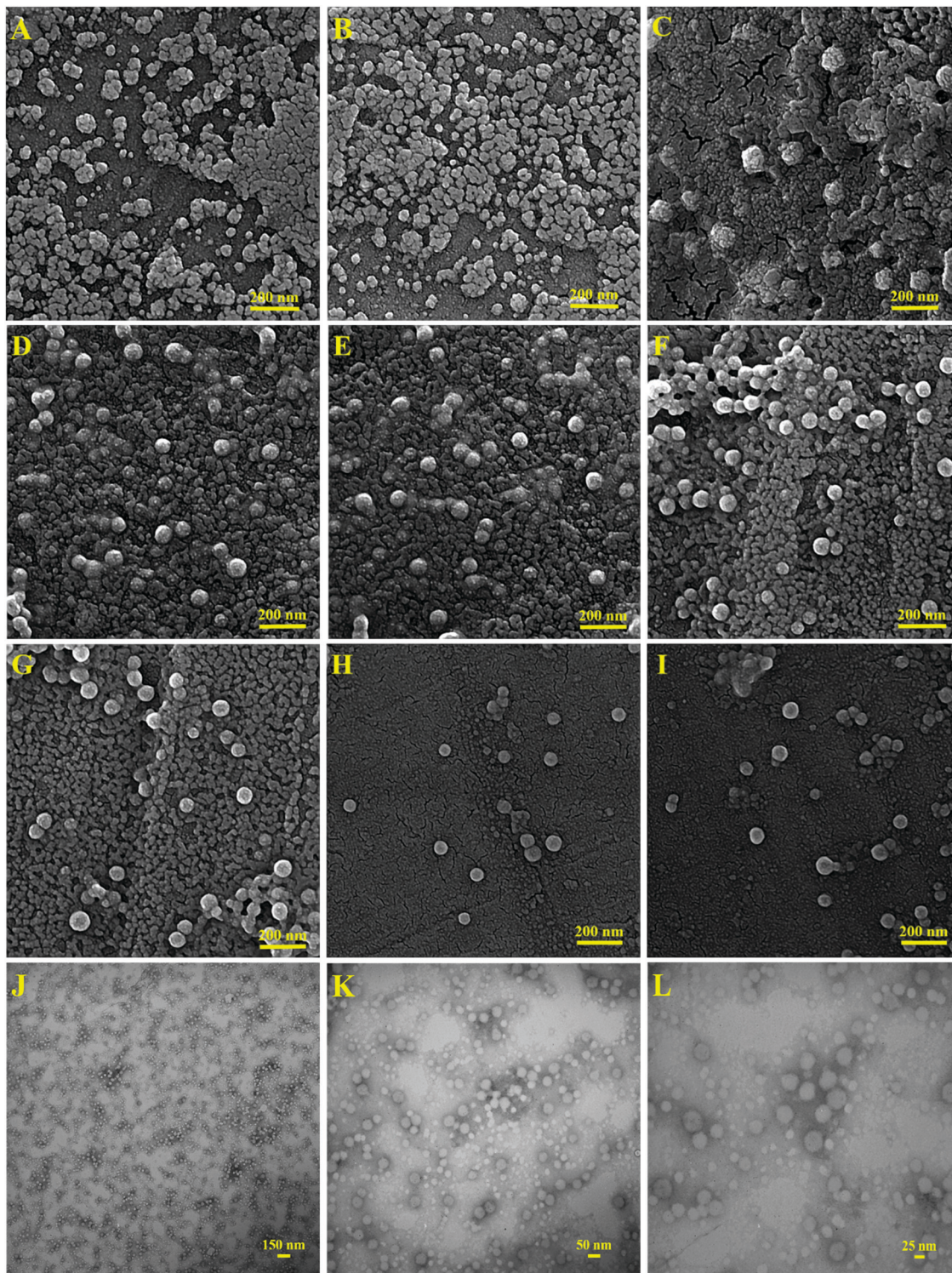


Fig. 4 SEM images for the stimuli-chromic latex nanoparticles: (A and B) PBA-SP, (C) PBAMMA-SP1, (D and E) PBAMMA-SP2, (F and G) PBAMMA-SP3, and (H and I) PMMA-SP. (J–L) TEM images of the stimuli-chromic latex nanoparticles (PMMA-SP) at different magnifications.

100 nm. The SEM images of the PBAMMA-SP2 (Fig. 4(D and E)), PBAMMA-SP3 (Fig. 4(F and G)), and PMMA-SP (Fig. 4(H and I)) samples display particle sizes below 100 nm with a narrow distribution. The contaminants observed in the background of the SEM images resulted from the phosphotungstic acid added to

the colloidal latex for decoration of the particles and increasing their stability upon electron beam irradiation. In addition, the size differences between the SEM and DLS results originate from the fact that the SEM sample was in the dry state, whereas the DLS sample was in the aqueous colloidal state. A brief comparison

between the SEM images of the stimuli-chromic latex samples displays that the nanoparticles were more stable with a decrease in the BA content and increase in  $T_g$ . The best SEM images with smooth spherical morphologies were observed for the PMMA-SP sample with a  $T_g$  of about 112 °C. To investigate the effect of spiropyran on particle morphology, the PMMA latex sample without spiropyran molecules was studied by SEM and the image is presented in Fig. S2 (see ESI†). The particle size and morphology of the PMMA and PMMA-SP samples were the same; therefore, spiropyran did not affect the size and morphology of the latex nanoparticles when used in a low content (1 wt%).

Fig. 4(J–L) display the TEM images of the PMMA-SP sample at different magnifications. This sample was selected because its high stability under the electron beam in the SEM analysis. Similar to the results from DLS and SEM, spherical nanoparticles with a narrow size distribution and mean particle size of about 50 nm were observed in the TEM images. As a result of their very low particle size and high surface area, it is expected that these stimuli-chromic latex nanoparticles will show interesting photochromic properties and also fluorescence emission even with the minimum spiropyran content (1 wt%). It should be noted that these properties can significantly be affected by the chain flexibility and polarity of the matrix. Thus, the investigation of these factors on the photochromism and fluorescence properties of the latex samples is presented in the follow section.

### 3.3. Photochromism and fluorescence emission of the stimuli-chromic latex nanoparticles

As shown in Fig. 1, some of the prepared stimuli-chromic latex nanoparticles show both photochromism and fluorescence characteristics upon UV irradiation. The turbidity of the latex samples is due to the dispersion of the latex nanoparticles in water and the resulting reflection of light. The PMMA-SP and BAMMA-SP3 samples displayed red fluorescence emission under UV light (365 nm) and also a change in color from white or light yellow to purple after UV illumination. Contrary to expectation, the latex nanoparticles with a higher BA content (PBA-SP, PBAMMA-SP1, and PBAMMA-SP2) showed weak coloration and also blue fluorescence emission under UV light. Apparently, an increase in photochromism and fluorescence emission intensities was observed with a decrease in  $T_g$  and increase of chain flexibility. Therefore, a factor besides the flexibility of the polymer chains controls the photochromism and responsivity of the spiropyran pendant groups. The isomerization of SP  $\leftrightarrow$  MC can significantly be affected by the polarity of the polymer chains and also media, where the MC form is stabilized as the quinoidal structure (QMC), protonated MC (MCH), and deprotonated MC in nonpolar, protic polar, and aprotic polar media.<sup>26,42</sup> BA in the structure of the copolymers can induce nonpolar behavior in the stimuli-chromic latex nanoparticles, which significantly influences the SP  $\leftrightarrow$  MC isomerization and also the related coloration and fluorescence emission.

To investigate the coloration and fluorescence emission upon UV irradiation observed in Fig. 1, the stimuli-chromic latex nanoparticles were analyzed by UV-Vis spectroscopy and

the results are presented in Fig. 5. For this, the latex samples were diluted from 10 to 0.3 wt% and then analyzed before and after UV (365 nm) illumination for 5 min. As shown in Fig. 5, the  $\lambda_{\max}$  and absorbance intensity of the samples display a relationship with the polarity of the polymer chains as a function of BA content. The difference between the  $\lambda_{\max}$  of the samples is attributed to the interactions of the MC molecules with the polymer chains and their effects on the ground-state energy gaps of the conjugated MC structure, which is well-known as hypsochromic (blue shift or decrease in  $\lambda_{\max}$  to a shorter wavelength or higher frequency) and bathochromic (red shift or increase in  $\lambda_{\max}$  to a longer wavelength or lower frequency) phenomena.<sup>26,42</sup> The hypsochromic shift was observed with a decrease in BA or increase in MMA content, where the minimum and maximum  $\lambda_{\max}$  (540 and 572 nm) were observed for the PMMA-SP and PBA-SP samples in Fig. 6(E) and (A), respectively. The other samples have  $\lambda_{\max}$  values between these two values (Fig. 6(B–D)). Hypochromism or decrease in absorbance intensity was observed with an increase in BA or decrease in MMA content as a result of the decrease in polarity. In contrast, hyperchromism or increase in absorbance intensity was shown with an increase in polymer chain polarity due to the increase in MMA content. The results shown in Fig. 5 clearly confirm that the photochromic properties of spiropyran are significantly influenced by the polarity of the polymer chain; however, chain flexibility does not play an important role. The MC form is a zwitterionic and highly-polar molecule stabilized by polar interactions, which leads to an increase in absorbance intensity and displacement of the  $\lambda_{\max}$  to shorter wavelengths. In contrast, the MC form is stabilized in non-polar media since the MCQ structure is characterized by a  $\lambda_{\max}$  close to 600 nm and minimum absorbance intensity.<sup>26,42</sup> An excessive increase in polarity (polar-polar and hydrogen bonding interactions) induced negative photochromism in the system, which is a known disadvantage of stimuli-chromic polymers. A clear relationship between the photochromism and polymer chain polarity was comprehensively investigated as hypsochromism/bathochromism for  $\lambda_{\max}$  changes and also hypochromism/hyperchromism for absorbance intensity variations. However, the different fluorescence emissions for the latex nanoparticles are not comprehensively discussed here, which was investigated by fluorescence spectroscopy.

Spiropyran as a photochromic compound displays photochromism and fluorescence emission *via* fast and reversible SP  $\leftrightarrow$  MC isomerization upon the absorption of UV irradiation (365 nm). The MC isomer shows red fluorescence with an emission peak in the range of 500–800 nm (see Fig. S3 (ESI†) for the PMMA-SP sample excited at 410 nm, which showed an emission peak at 715 nm), which can be influenced by the polarity and pH of the medium. Here, the fluorescence emission of the latex samples was investigated to determine the main reason for the different fluorescent emissions observed in Fig. 1. For this, diluted latex samples with a concentration of 0.3 wt% were used to investigate their emission by fluorescence spectroscopy under an excitation wavelength of 360 nm. Fig. 6 displays the fluorescence spectra for the stimuli-chromic latex nanoparticles, which have different fluorescence emissions under UV irradiation. Each sample showed an emission peak in the



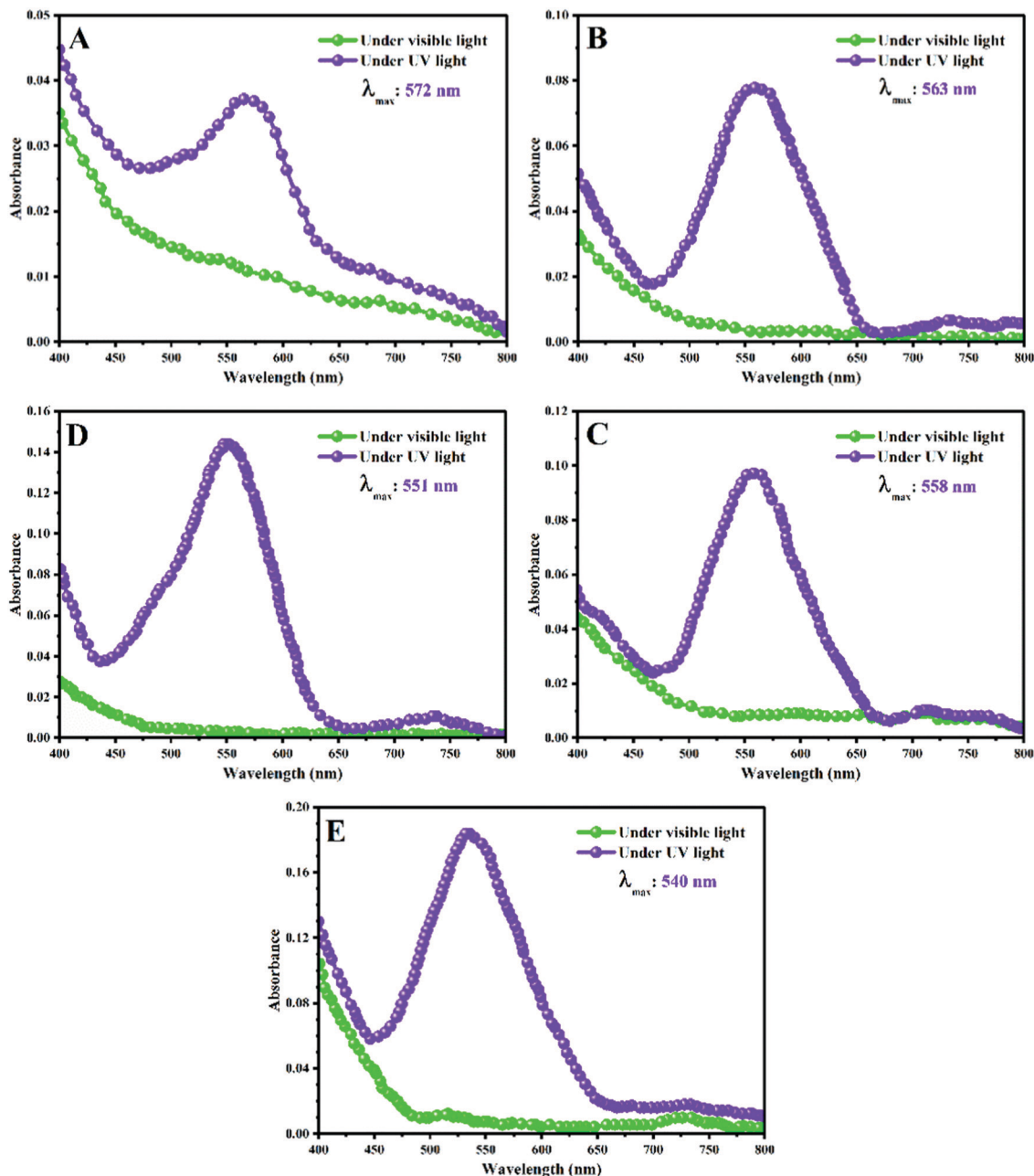


Fig. 5 UV-Vis spectra of the stimuli-chromic latex nanoparticles (with a solid content of about 0.3 wt%) before and after UV illumination (365 nm): (A) PBA-SP, (B) PBAMMA-SP1, (C) BAMMA-SP2, (D) PBAMMA-SP3, and (E) MMA-SP.

wavelength range of 390–430 nm with different fluorescence intensities. As shown in Fig. 6, the fluorescence intensity increased with a decrease in the BA content in the copolymer structure. According to the discussion reported for the effect of polymer chain polarity on the photochromism of spirocyan, the increase in fluorescence intensity can be attributed to the increase of polymer chain polarity because of the higher polarity of MMA in comparison with BA. The fluorescence peaks of PBA-SP (Fig. 6(A)), PBAMMA-SP1 (Fig. 6(B)), PBAMMA-SP2 (Fig. 6(C)), and PBAMMA-SP3 (Fig. 6(D)) are very broad, which may result from the overlapping of some peaks. The two peaks observed in the fluorescence spectrum of PMMA-SP in Fig. 6(E) confirm this

claim. The broad emission peaks are due to the presence of more than one isomer for the MC molecule, such as the MCQ isomer, which is stable in non-polar media. This was further confirmed by the two peaks observed for PMMA-SP in Fig. 6E (397 and 415 nm). Therefore, the red fluorescence emission observed for the PMMA-SP and PBAMMA-SP3 samples resulted from the MC isomer. However, the blue emission for the PBA-SP, PBAMMA-SP1, and PBAMMA-SP2 samples is due to the presence of the MCQ isomer in the non-polar medium, as shown in Fig. 5. In summary, the photochromic properties and fluorescence emission of the spirocyan chromophore are mainly affected by the polarity of the polymer chains, as confirmed by the bright red

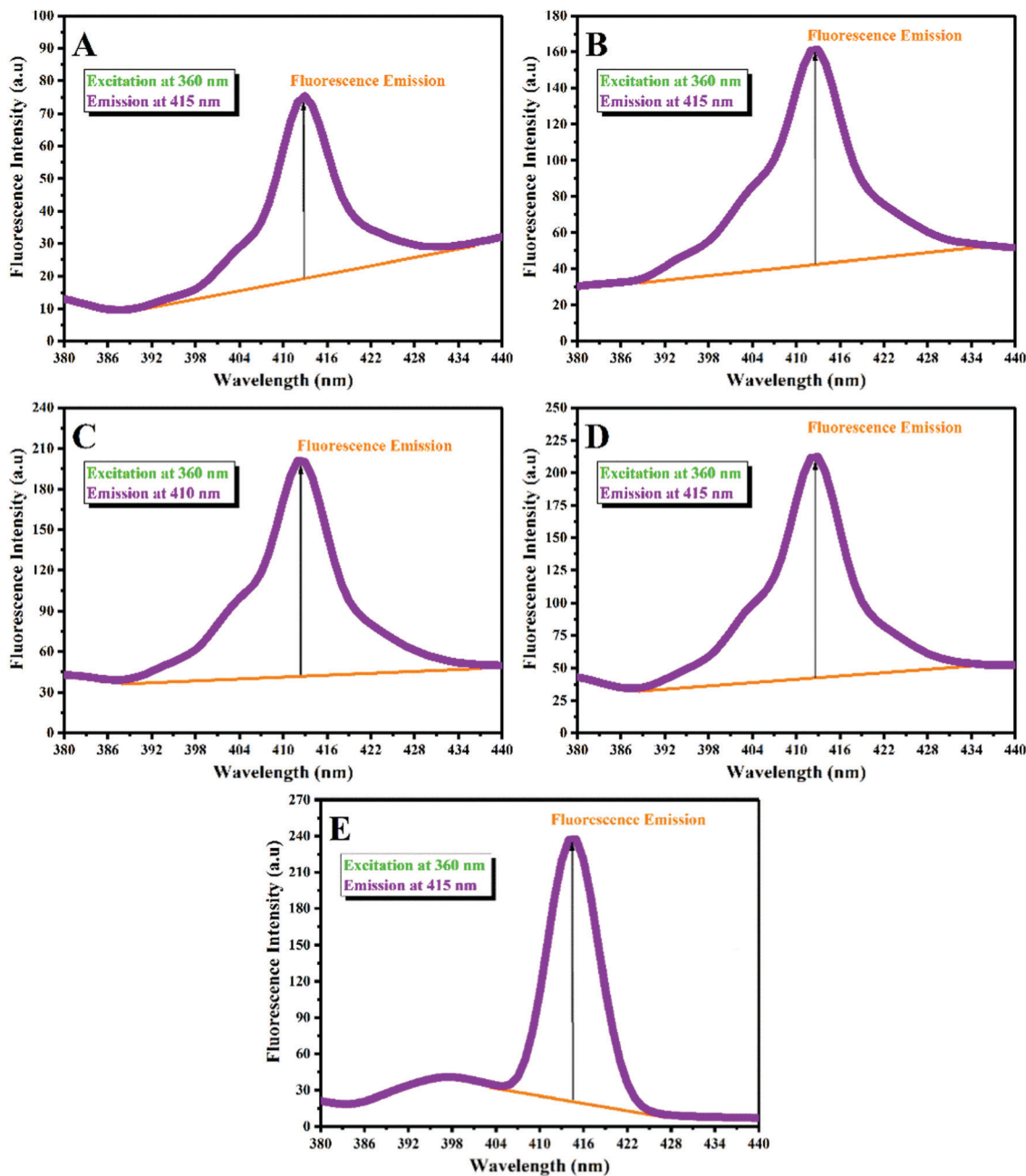


Fig. 6 Fluorescence emission spectra of the stimuli-chromic latex nanoparticles (with a solid content of about 0.3 wt%) excited at the wavelength of 360 nm: (A) PBA-SP, (B) PBAMMA-SP1, (C) PBAMMA-SP2, (D) PBAMMA-SP3, and (E) PMMA-SP.

fluorescence emission and also photochromism with high intensity for the PMMA-SP sample. To clarify the color differences between the samples before and after UV irradiation, all the samples were investigated by CIE position color analysis by measurement of the  $L^*$ ,  $a^*$ , and  $b^*$  parameters (see Table S2 in the ESI<sup>†</sup>). Then, these values were used to determine  $\Delta E^*$  (indicate the color difference before and after UV irradiation) and also the CIE 1931 chromaticity diagrams, as shown in Fig. S4 (ESI<sup>†</sup>). The results indicate that the maximum color change was observed for the PMMA-SP sample, according to Fig. S4-E and its maximum  $\Delta E^*$  in Table S2 (ESI<sup>†</sup>). This strongly confirms the photochromism and photoluminescence characteristics obtained

by UV-Vis and fluorescence spectroscopy, respectively. In addition, the kinetics of the SP  $\leftrightarrow$  MC isomerization and photofatigue resistance of the samples were investigated because of their importance in anticounterfeiting applications.

The responsivity of the stimuli-chromic latex samples to UV and visible light is significant for their application in anti-counterfeiting inks, which was investigated by monitoring the kinetics of the SP  $\leftrightarrow$  MC isomerization. After printing security marks on a document, the anticounterfeiting ink should display photochromism and fluorescence emission upon UV illumination in a fast and reversible manner. Therefore, investigation of the kinetics of the SP  $\leftrightarrow$  MC isomerization for all the samples

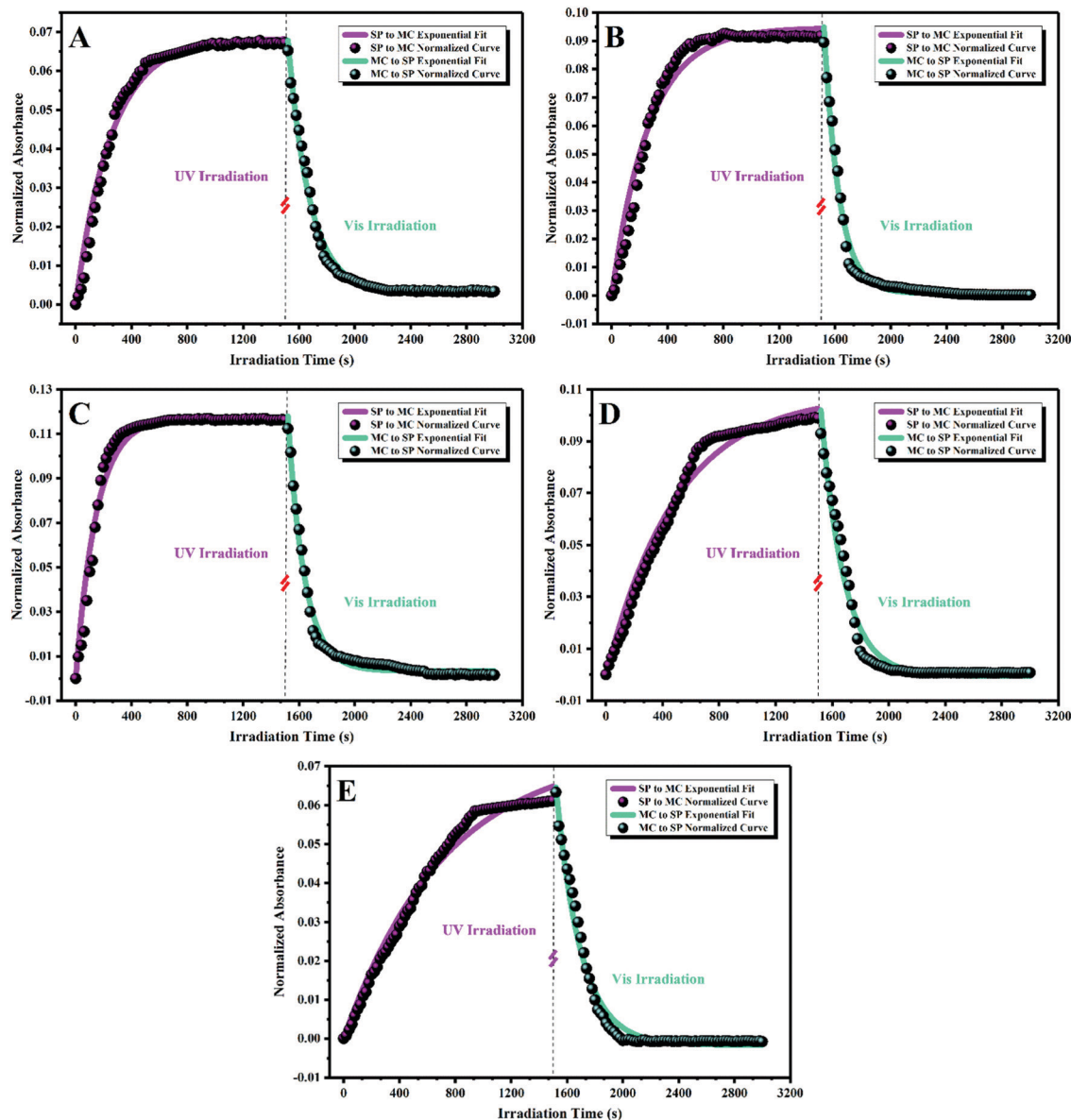


Fig. 7 Normalized and exponential fitting curves of the SP to MC and MC to SP isomerization kinetics for the stimuli-chromic latex nanoparticles at the corresponding  $\lambda_{\text{max}}$  under UV and visible light irradiation: (A) PBA-SP, (B) PBAMMA-SP1, (C) PBAMMA-SP2, (D) PBAMMA-SP3, and (E) PMMA-SP.

containing spiropyran photoswitches by UV-Vis spectroscopy was necessary. The kinetics of the SP  $\leftrightarrow$  MC isomerization was investigated by exposing the diluted latex samples with a solid content of about 0.3 wt% to UV (wavelength of 365 nm) and visible light irradiation at different irradiation time intervals (20 s) and measurement of the absorbance at specific  $\lambda_{\text{max}}$  by UV-Vis spectroscopy. Then, the measured absorbance values were normalized with respect to the absorbance of each sample before UV and visible light irradiation. The normalized results were plotted as a function of irradiation time to obtain the kinetic curves for the SP  $\leftrightarrow$  MC isomerization reactions, as shown in Fig. 7. To extract the kinetic equations and parameters ( $k_c$  and  $T_{1/2}$ ), the Origin software (Professional 2017) was used for fitting the resulting data with suitable curves. For this, the SP to MC isomerization kinetics was fitted using the BoxLucas1 model, and the MC to SP

isomerization (back reaction) was fitted using the ExpDec1 model, according to eqn (1) and (2), respectively.

$$\frac{\text{Normalized absorbance}(t)}{\text{Normalized absorbance}(\infty)} = A(1 - \exp(-k_{c1}t)) \quad (1)$$

$$\frac{\text{Normalized absorbance}(t)}{\text{Normalized absorbance}(\infty)} = A_0 + A \exp(-k_{c2}t) \quad (2)$$

where,  $A$  and  $A_0$  are the constant values and  $k_{c1}$  and  $k_{c2}$  represent the rate constants for the SP to MC (eqn (1)) and MC to SP (eqn (2)) photoisomerization upon UV and visible light irradiation, respectively. The normalized absorbance values at time  $t$  and  $\infty$  were extracted from Fig. 7. It should be noted that  $k_c$  and  $T_{1/2}$  are significant parameters for monitoring the photoresponsivity of the photochromic latex samples to UV and visible light

Table 1 SP to MC and MC to SP isomerization rate equations and the corresponding kinetic parameters for the stimuli-chromic latex samples

Sample	SP to MC			MC to SP				
	Equation	$R^2$	$k_{c1}$ ( $s^{-1}$ )	$T_{1/2}^a$ (s)	Equation	$R^2$	$k_{c2}$ ( $s^{-1}$ )	$T_{1/2}^a$ (s)
PBA-SP	$0.068 - 0.068 \times \exp(-0.004t)$	0.98	0.004	174	$1.07 \times 10^{-4} + (1294 \times \exp(-0.0064t))$	0.99	0.0064	129
PBAMMA-SP1	$0.095 - 0.095 \times \exp(-0.0038t)$	0.97	0.0038	183	$4.18 \times 10^{-3} + (42\,600 \times \exp(-0.0084t))$	0.99	0.0084	106
PBAMMA-SP2	$0.117 - 0.117 \times \exp(-0.0067t)$	0.97	0.0067	102	$1.26 \times 10^{-3} + (122\,104 \times \exp(-0.0092t))$	0.98	0.0092	96
PBAMMA-SP3	$0.108 - 0.108 \times \exp(-0.002t)$	0.98	0.002	323	$6.29 \times 10^{-4} + (1378 \times \exp(-0.0062t))$	0.98	0.0062	132
PMMA-SP	$0.0742 - 0.0742 \times \exp(-0.0014t)$	0.98	0.0014	416	$-3.18 \times 10^{-4} + (389.69 \times \exp(-0.0056t))$	0.98	0.0056	142

<sup>a</sup> The time required to reach half of the final absorbance for the coloration.

irradiation. Similarly to the results observed for the photochromic behavior of the samples in Fig. 5, different kinetic curves and parameters were observed for each of the samples in Fig. 7 and Table 1. This resulted from the effect of the polymer chain polarity and flexibility ( $T_g$ ) on the stabilization of the MC and SP forms. Fig. 7 shows the kinetic curves for the SP  $\leftrightarrow$  MC photoisomerization and also the fitted equations with excellent  $R^2$  values (0.97–0.99). In addition, the kinetic parameters ( $k_c$  and  $T_{1/2}$ ) extracted from the curves are presented in Table 1. According to the recent studies,<sup>24,25</sup> the kinetic parameters showed significant dependency on the polarity and flexibility of the polymer chains in the latex samples. This is a result of the interactions between the polymer chains with the SP and MC molecules, and the free volume in the flexible polymers for the acceleration of SP  $\leftrightarrow$  MC isomerization. An increase in the polarity of the polymer chains resulted in an increase in the rate of SP to MC isomerization (maximum  $k_c$  and minimum  $T_{1/2}$ ) and decrease in the rate of MC to SP isomerization (minimum  $k_c$  and maximum  $T_{1/2}$ ). Correspondingly, a decrease in the polarity resulted in slower SP to MC isomerization and also faster MC to SP isomerization. This is due to the high stability of the polar zwitterionic MC structure in polar media and high stability of the SP form in nonpolar media. Chain flexibility in addition to polarity plays also a key role, where an increase in flexibility can accelerate both the SP to MC and MC to SP isomerizations. The results in Table 1 show that kinetic parameters are affected by both the polarity and flexibility of the polymer chains. An increase in the SP  $\leftrightarrow$  MC isomerization rate was observed for the PBAMMA-SP2 sample (maximum  $k_{c1}$  and  $k_{c2}$ , minimum  $T_{1/2}$  for both the SP to MC and MC to SP isomerizations) compared to the PBA-SP and PBAMMA-SP1 samples due to the increase in polarity (higher MMA content). An interesting trend was observed for the SP  $\leftrightarrow$  MC isomerization by comparing the kinetic parameters of PBAMMA-SP2 with both the PBAMMA-SP3 and PMMA-SP samples, where the PBAMMA-SP2 sample showed a high rate for the SP to MC and MC to SP isomerizations (maximum  $k_{c1}$  and  $k_{c2}$  and minimum  $T_{1/2}$  for both the SP to MC and MC to SP isomerizations). Flexibility is the main reason for this trend because an increase in polarity results in faster SP  $\leftrightarrow$  MC isomerization for the PMMA-SP sample. Thus, the kinetic studies show that both polarity and flexibility of the polymer chains are significant parameters in the light-responsivity of spiropyran in the stimuli-chromic latex nanoparticles. The fast SP  $\leftrightarrow$  MC isomerization was observed for the PBAMMA-SP2 sample with medium polarity (67 wt% of MMA and 33 wt% of

BA in the feed) and flexibility ( $T_g$  of about 33 °C) of the polymer chains. There are some factors for the selection of a stimuli-chromic latex sample as an anticounterfeiting ink. For example, photochromism and fluorescence emission with high intensity (MMA-SP is interesting), fast light-responsivity (BAMMA-SP2 is interesting), photofatigue resistance and stability on cellulosic matrix. Thus, for the selection of the best sample, the photofatigue resistance and stability on cellulosic paper was investigated for the stimuli-chromic latex samples.

Photostability, reversibility, and photoswitchability under alternating UV/visible light irradiation cycles or in a long time period are the most significant challenges in the development of advanced materials based on photochromic compounds.<sup>25,63,64</sup> Thus, these properties were investigated by photofatigue resistance analysis, where the absorbance intensity was measured after each UV/visible irradiation cycle several times. For this, all the diluted stimuli-chromic latex samples with a solid content of about 0.3 wt% were exposed to UV or visible light irradiation for 5 min, and their absorbance in a specific  $\lambda_{max}$  was measured by UV-Vis spectroscopy in more than 20 cycles to obtain the photofatigue-resistance curves. It should be noted that the standard cycles for this behavior is 10–15, which was set to 20 cycles here because of the importance of photofatigue resistance in anticounterfeiting materials. The samples were exposed to visible light and UV illumination, and the absorbance values at the corresponding  $\lambda_{max}$  (according to the reported values in Fig. 5) were measured for each sample and plotted against cycle number, as shown in Fig. 8. The results display that the photochromic properties of the latex nanoparticles are fully reversible over a long period or several UV/visible light irradiation cycles, which is strong confirmation of the photoswitchability of the color and fluorescence emission of the spiropyran molecules in the latex nanoparticles. Hydrophobic polymer nanoparticles are a significant tool for the protection of spiropyran toward environmental degradation and especially negative photochromism in polar media such as water, where suitable photoswitchability and photofatigue resistance display their efficient role. Thus, to choose the best sample for the preparation of anticounterfeiting inks, it was necessary to investigate the stability of the latex nanoparticles on the surface of paper and tissue.

### 3.4. Incorporation of the latex nanoparticles in cellulosic paper and cotton tissue

In the development of anticounterfeiting inks using the spiropyran-containing stimuli-chromic latex samples for security printing and

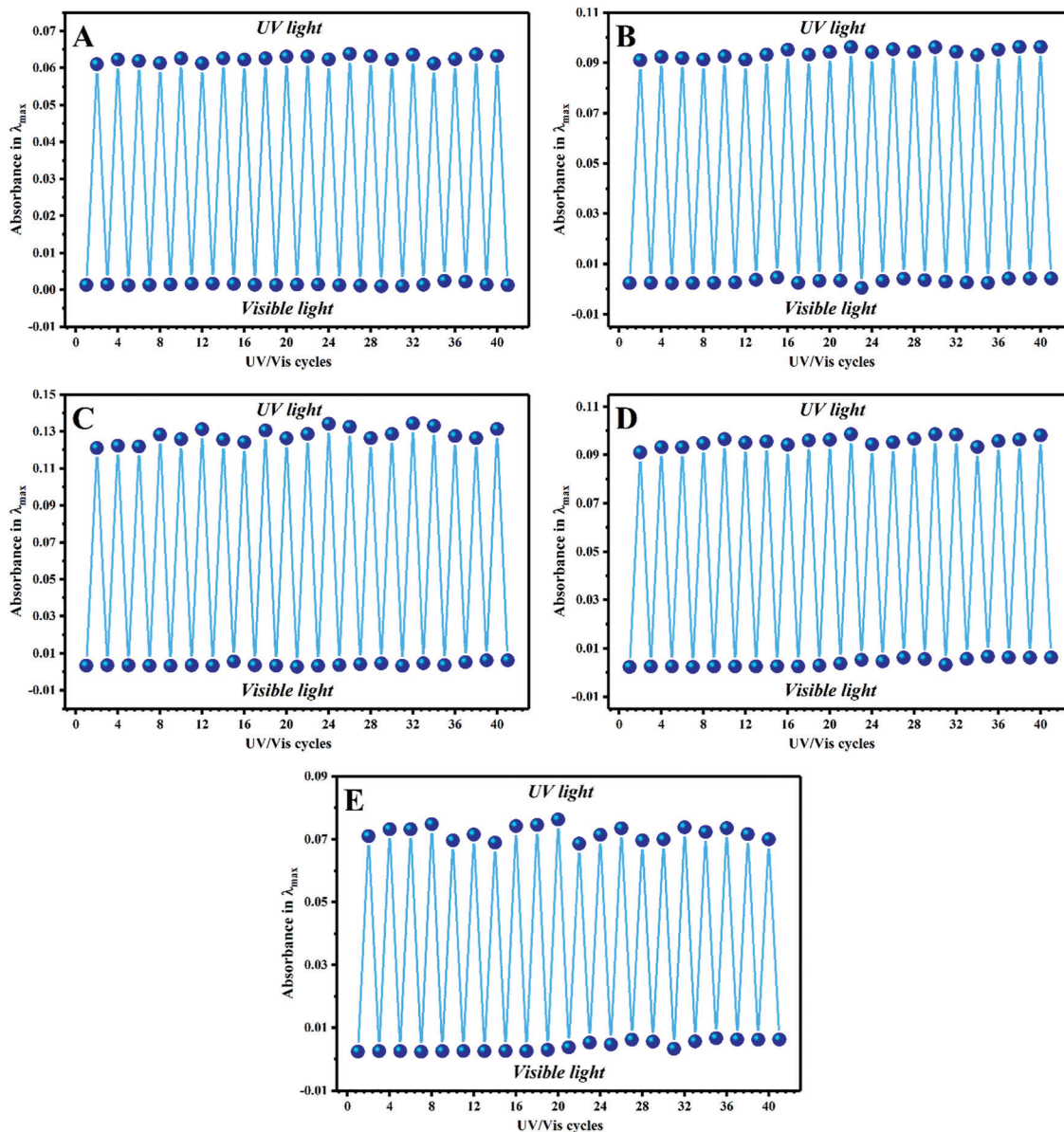


Fig. 8 Photofatigue-resistance characteristics of the stimuli-chromic latex samples upon alternating UV (365 nm for 5 min) and visible light (5 min) irradiation: (A) PBA-SP, (B) PBAMMA-SP1, (C) PBAMMA-SP2, (D) PBAMMA-SP3, and (E) PMMA-SP.

marking on cellulosic substrates, coating of the nanoparticles and their stability on the cellulosic surface are significant parameters, which are remarkably affected by the morphology and flexibility of the nanoparticles. Thus, cellulosic papers and cotton tissues impregnated with PBA-SP and PMMA-SP latex samples were prepared, and the SEM images of the surface of these papers and tissues are shown in Fig. 9. For this, some pieces of cellulosic paper and cotton tissue were soaked in the latex samples for 1 min, dried at 40 °C for 1 h, and directly used for SEM imaging after depositing a gold layer. The smooth fibers of the cellulosic paper and cotton tissue were observed without any additional layers on their surface, as shown in Fig. 10(A–A') and (B–B'), respectively. After incorporation of the latex nanoparticles, the surface morphology of the cellulose and cotton fibers varied. The surface morphology of the cellulose and tissue fibers after treatment with

the PBA-SP latex sample is shown in Fig. 10(C–C') and (D–D'), respectively. Accordingly, the nanoparticles showed a uniform film with high stability on the cellulose and cotton fibers because of their small particle size (below 100 nm) and the high flexibility of the polymer chains. Fig. 10(C') and (D') show the formation of a very smooth layer of stimuli-chromic latex nanoparticles on the surface of the cellulose and cotton fibers due to their physical adsorption, which is a significant advantage for the stability of the anticounterfeiting inks on cellulosic and cotton substrates. Fig. 10(E–E') show the appropriate coating of the cellulosic paper with the PMMA-SP sample, which is a result of the spherical morphology of the nanoparticles and hydrogen bonding between the hydroxyl groups of cellulose with the polar functionalities of MMA. Similar results were observed for the impregnated cotton fibers with the PMMA-SP latex sample in Fig. 10(F–F').

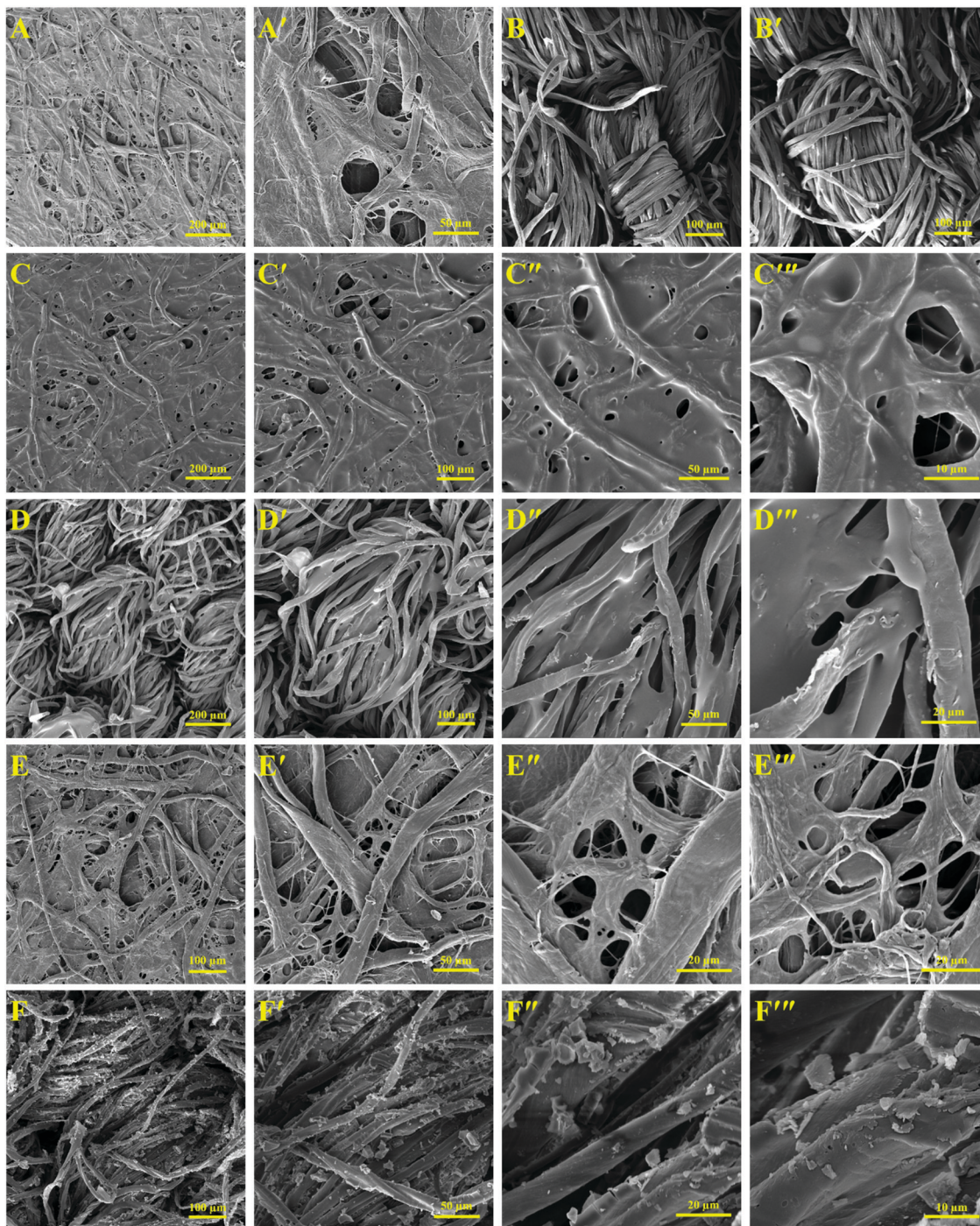


Fig. 9 SEM images of the impregnated cellulosic paper and tissue with the spirocyan-modified latex particles: (A and A') neat cellulosic paper, (B and B') neat cotton tissue, (C–C''') impregnated cellulosic paper with PBA-SP, (D–D''') impregnated cotton tissue with PBA-SP, (E–E''') impregnated cellulosic paper with PMMA-SP, and (F–F''') impregnated cotton tissue with PMMA-SP.

Furthermore, the impregnated cellulosic papers were used to investigate the stability and printability of the latex samples on the paper surface by measurement of the contact angle before and after UV irradiation, as shown in Fig. S5 (ESI<sup>†</sup>). The papers impregnated with PBA-SP (Fig. S5-A, ESI<sup>†</sup>) and PMMA-SP (Fig. S5-C, ESI<sup>†</sup>) showed contact angles of about 90° and 77° before UV irradiation, respectively. After UV illumination

(365 nm, 5 min), these values decreased to 80° and 65° for the PBA-SP and PMMA-SP samples, respectively, as a result of the isomerization of the nonpolar SP molecules to the highly polar MC molecules. This is an interesting confirmation of the stability and printability of the latex nanoparticles on cellulosic paper, where the higher contact angle for the impregnated paper with PBA-SP latex is due to the lower polarity (higher hydrophobicity) of PBA in comparison



Fig. 10 Application of the stimuli-chromic latex nanoparticles (PMMA-SP) as an anticounterfeiting and rewritable ink for print-marking on security documents.

with PMMA. The UV-Vis and fluorescence spectroscopy results of the latex samples in combination with the SEM and contact angle images of the impregnated cellulosic materials display that PMMA-SP is the most appropriate latex sample for the development of anticounterfeiting inks because it showed (I) high UV absorbance (Fig. 5(E)) with no negative photochromism, (II) high-intensity color change (photochromism) and fluorescence emission upon UV light irradiation (Fig. 1), (III) suitable kinetic parameters for the SP  $\leftrightarrow$  MC isomerization and high photoswitchability, reversibility, and photofatigue resistance, and (IV) interesting surface coating and stability after its incorporation on the cellulosic matrix. Therefore, the PMMA-SP sample was selected for the preparation of a photochromic and fluorescent anticounterfeiting ink for use in high-security print-marking and rewritable photopatterning on cellulosic paper.

### 3.5. High-security anticounterfeiting print-marking and rewritable photopatterning

Increasing the security of anticounterfeiting inks has become a highly significant challenge because of the high incidents of copying and counterfeiting of security documents, which can be solved by using photochromic/fluorescent nanoparticles as high-security anticounterfeiting materials.<sup>11,56,57,65,66</sup> The PMMA-SP sample, because of its most suitable photochromism, fluorescence, reversibility, photofatigue resistance, and stability on cellulosic paper, was used in the preparation of a photochromic and fluorescent anticounterfeiting ink for use in high-security print-marking and erasable photopatterning. The anticounterfeiting ink prepared from the PMMA-SP latex sample was loaded to stamps with specific marks such as quick a response code (QR), barcode, some schemes related to the SP and MC structures, and some words (security, photochrom, and spiropyran). All the stamps were used for print-marking on a model security document (certificate) and the color change of the printed marks was investigated after UV irradiation by photography, as shown in Fig. 10. The print-marked document exhibited some invisible marks under white light, which became visible upon UV irradiation (365 nm) *via* the isomerization of SP to

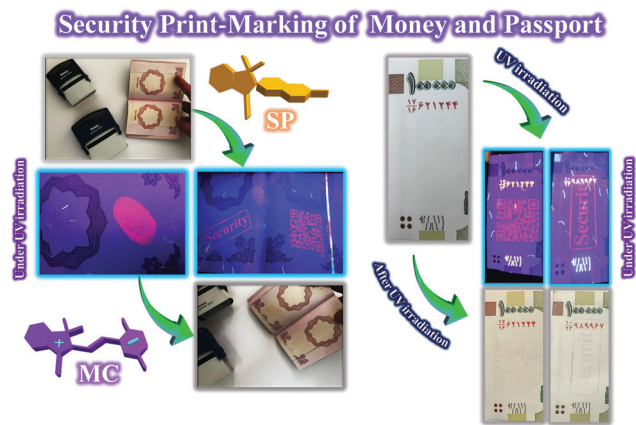


Fig. 11 Security print-marking on money and passport using different stamps loaded with the photochromic and fluorescent anticounterfeiting ink based on PMMA-SP.

the MC form. For instance, QR and barcode marks can be prepared for a person or brand, which can be characterized by QR and barcode reader instruments after irradiation of the document with UV light and visibility of the security QR and barcode from colorless to purple. In addition, a red fluorescence emission was observed for the printed marks under UV irradiation. Anticounterfeiting stamps are a fast and facile tool for security marking on different documents using of photochromic and fluorescent latex nanoparticles as anticounterfeiting invisible inks.

Money, passports, and national cards are important security documents, which require inhibition from copying and counterfeiting. Thus, the use of high-security anticounterfeiting inks with photochromism and fluorescence emission is a powerful solution in the current study for problems related to the copying and counterfeiting of security documents. Therefore, anticounterfeiting stamps loaded with the PMMA-SP latex ink were used for printing different security marks on money and a passport. The photochromism and fluorescence characteristics of the printed marks were investigated under and after UV irradiation (365 nm), and the photos are presented in Fig. 11. The printed marks on the money and passport displayed a highly intense and luminous red fluorescence emission under UV light, where the invisible marks in white light were converted to visible purple marks after UV irradiation. In addition, the prepared anticounterfeiting ink was used for application of a finger-print on a passport, which was invisible under white light and converted to visible purple sign after UV irradiation in addition to its highly intense and luminous red fluorescence emission under UV light. The high-security of this anticounterfeiting ink is due to its simultaneous display of both photochromism and fluorescence emission security characteristics, which is very important for increasing the safety and reducing counterfeiting in different security documents. The fast coloration and fluorescence emission, long lifetime, high photofatigue resistance, high stability on cellulosic papers, reversibility, photoswitchability, and facile preparation method are some of the unique advantages of this photochromic and fluorescent anticounterfeiting ink.

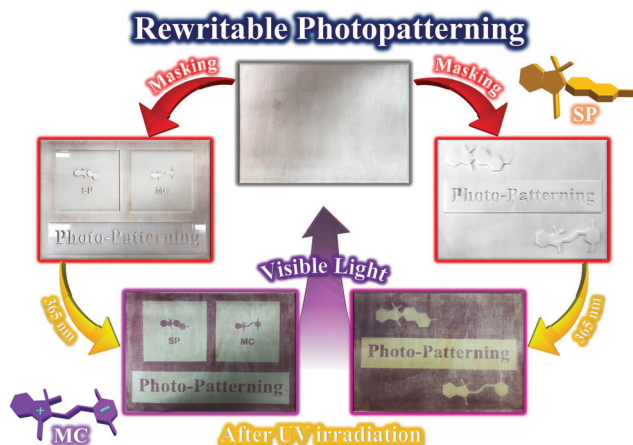


Fig. 12 Coating of the stimuli-chromic latex nanoparticles (PMMA-SP) on cellulose paper and investigation of rewritable photopatterning.

Photopatterning is a significant application of photochromic and fluorescent latex nanoparticles containing spiropyran photoswitches. The development of photochromic and fluorescent latex nanoparticles with the ability to induce photopatterns on different substrates has been an important challenge in recent decades. Cellulose paper is among the most significant substrates for the preparation of photopatterns by its coating with stimuli-chromic polymers. The PMMA-SP sample is a photochromic and fluorescent latex composed of spherical polymer nanoparticles bearing spiropyran photoswitches. The polarity of the MMA units and particle size below 100 nm offer high coating ability to the latex nanoparticles and their stability on cellulose paper, as shown in Fig. 9. Therefore, erasable and rewritable cellulose photopatterns were prepared by spraying of the PMMA-SP latex (10 wt%) on the surface of paper and drying at 45 °C. The resulting papers were exposed to UV irradiation under different masks for 1 min, and colored photopatterns could clearly be observed after removal of the mask, as shown in Fig. 12. This photopatterning was fully reversible under alternating UV/visible light irradiation cycles for several times. The rewritable cellulose photopatterns were initially discolored, where coloration occurred immediately upon UV irradiation (365 nm). Thus, the use of spiropyran-containing stimuli-chromic latex samples is an efficient, fast, and facile method for the preparation of photochromic and fluorescent photopatterns based on cellulose paper. Future studies should be conducted using of the most flexible stimuli-chromic latex nanoparticles (for example BAMMA-SP2) for the preparation of anticounterfeiting materials to show photochromism and fluorescence emission with high intensity upon UV irradiation in addition to fast-responsivity, reversibility, and photofatigue resistance.

## 4. Conclusion

Invisible and flexible photochromic/photoluminescent anticounterfeiting ink with high-security was developed *via* the synthesis of stimuli-chromic latex nanoparticles with different  $T_g$  values *via* the semi-continuous mini-emulsion copolymerization of MMA, BA, and

SPEA. The flexibility of the copolymers was studied by measuring their  $T_g$  from the DSC thermograms. There was no significant difference between the theoretical and experimental  $T_g$  values. The DLS, SEM, and TEM results display spherical particles with a size of 50–80 nm and narrow distribution. The investigation of photochromic properties and fluorescence emission displayed that the polarity and flexibility of the polymer chains affect the optical properties, where different photochromism and fluorescence emissions were observed for the latex samples upon UV illumination. On the other hand, the kinetic investigation of the SP  $\leftrightarrow$  MC isomerization showed that PBAMMA-SP2 with medium flexibility ( $T_g$  of 33 °C) and polymer chain polarity (67 wt% of MMA and 33 wt% of BA) displayed fast photoresponsivity toward UV and visible light. However, the results of the CIE colorimetric analysis and UV-Vis and fluorescence spectroscopy indicated that the PMMA-SP sample has highly intense photochromism or color change, bright red fluorescence, photoswitchability, and photofatigue resistance without negative photochromism. The SEM images and contact angle results obtained from the cellulose paper and cotton tissue impregnated with the PBA-SP (highly flexible) and PMMA-SP (highly brittle) samples displayed the high surface coating, printability and stability of the nanoparticles on the cellulose and cotton fibers, where the most smooth surface was observed for the substrate impregnated with PBA-SP. Because of the importance of photochromism and fluorescence emission intensity for the final advanced application, the PMMA-SP sample was selected for the formulation of high-security photochromic/photoluminescent anticounterfeiting ink and spraying on cellulose paper to investigate its use in rewritable photopatterning. The prepared ink was loaded on different stamps and then applied on security documents (certificate, money, and passport) for print-marking with the aid of photochromic and fluorescent labeling. In addition, it was used for the induction of a fingerprint on a passport as a significant security mark. The printed marks displayed photochromism (colorless to purple) and bright red fluorescence emission after and under UV illumination (365 nm), respectively. Rewritable photopatterning of the cellulose paper was carried out by UV illumination under different masks, where the colored patterns were rapidly erasable by the induction of visible light or heat. Finally, a highly efficient strategy was developed for preparation of high-security photochromic/photoluminescent anticounterfeiting inks by using spiropyran photoswitches, where the print-marked documents displayed high security due to simultaneous presentation of photochromism and fluorescence emission upon UV irradiation.

## Conflicts of interest

The authors declare that there is no conflict of interest regarding publication of this paper.

## Acknowledgements

Iran National Science Foundation (INSF) is greatly appreciated for its financial support (Grant Number: 97003824).



## References

- 1 T. Han, Y. Yuan, X. Liang, Y. Zhang, C. Xiong and L. Dong, *J. Mater. Chem. C*, 2017, **5**, 4629–4635.
- 2 D. S. Puperi, R. W. O'Connell, Z. E. Punske, Y. Wu, J. L. West and K. J. Grande-Allen, *Biomacromolecules*, 2016, **17**, 1766–1775.
- 3 C. Sun, Z. Gao, H. Liu, L. Wang, Y. Deng, P. Li, H. Li, Z. H. Zhang, C. Fan and W. Bi, *Chem. Mater.*, 2019, **31**, 5116–5123.
- 4 S. Halivni, S. Shemesh, N. Waiskopf, Y. Vinetsky, S. Magdassi and U. Banin, *Nanoscale*, 2015, **7**, 19193–19200.
- 5 G. H. Lee, T. Y. Jeon, J. Bin Kim, B. Lee, C. S. Lee, S. Y. Lee and S. H. Kim, *Chem. Mater.*, 2018, **30**, 3789–3797.
- 6 C. Zhang, B. Wang, W. Li, S. Huang, L. Kong, Z. Li and L. Li, *Nat. Commun.*, 2017, **8**, 1138.
- 7 C. Sun, S. Su, Z. Gao, H. Liu, H. Wu, X. Shen and W. Bi, *ACS Appl. Mater. Interfaces*, 2019, **11**, 8210–8216.
- 8 K. Huang, N. M. Idris and Y. Zhang, *Small*, 2016, **12**, 836–852.
- 9 J. Zhang, F. Song, Z. He, Y. Liu, Z. Chen, S. Lin, L. Huang and W. Huang, *Small*, 2016, **12**, 397–404.
- 10 C. Chen, Y. Yu, C. Li, D. Liu, H. Huang, C. Liang, Y. Lou, Y. Han, Z. Shi and S. Feng, *Small*, 2017, **13**, 1702305.
- 11 H. Kang, J. W. Lee and Y. Nam, *ACS Appl. Mater. Interfaces*, 2018, **10**, 6764–6771.
- 12 A. F. Smith, P. Patton and S. E. Skrabalak, *Adv. Funct. Mater.*, 2016, **26**, 1315–1321.
- 13 K. Park, K. Jung, S. J. Kwon, H. S. Jang, D. Byun, I. K. Han and H. Ko, *Adv. Funct. Mater.*, 2016, **26**, 7836–7846.
- 14 K. Chang, Z. Liu, H. Chen, L. Sheng, S. X. A. Zhang, D. T. Chiu, S. Yin, C. Wu and W. Qin, *Small*, 2014, **10**, 4270–4275.
- 15 H. Q. Peng, C. L. Sun, L. Y. Niu, Y. Z. Chen, L. Z. Wu, C. H. Tung and Q. Z. Yang, *Adv. Funct. Mater.*, 2016, **26**, 5483–5489.
- 16 A. Abdollahi, H. Roghani-Mamaqani and B. Razavi, *Prog. Polym. Sci.*, 2019, **98**, 101149.
- 17 A. Abdollahi, H. Roghani-Mamaqani, A. Herizchi, H. Alidaei-Sharif, A. Enayati and S. Sajedi-Amin, *Polym. Chem.*, 2020, DOI: 10.1039/d0py00078g.
- 18 K. Jiang, Y. Wang, C. Cai and H. Lin, *Chem. Mater.*, 2017, **29**, 4866–4873.
- 19 Z. Song, T. Lin, L. Lin, S. Lin, F. Fu, X. Wang and L. Guo, *Angew. Chem., Int. Ed.*, 2016, **55**, 2773–2777.
- 20 K. Jiang, L. Zhang, J. Lu, C. Xu, C. Cai and H. Lin, *Angew. Chem., Int. Ed.*, 2016, **55**, 7231–7235.
- 21 D. Zhou, D. Liu, W. Xu, X. Chen, Z. Yin, X. Bai, B. Dong, L. Xu and H. Song, *Chem. Mater.*, 2017, **29**, 6799–6809.
- 22 A. Abdollahi, H. Roghani-Mamaqani, B. Razavi and M. Salami-Kalajahi, *Polym. Chem.*, 2019, **10**, 5686–5720.
- 23 A. Abdollahi, A. R. Mahdavian and H. Salehi-Mobarakeh, *Langmuir*, 2015, **31**, 10672–10682.
- 24 A. Abdollahi, K. Sahandi-Zangabad and H. Roghani-Mamaqani, *Langmuir*, 2018, **34**, 13910–13923.
- 25 A. Abdollahi, K. Sahandi-Zangabad and H. Roghani-Mamaqani, *ACS Appl. Mater. Interfaces*, 2018, **10**, 39279–39292.
- 26 A. Abdollahi, A. Mouraki, M. H. Sharifian and A. R. Mahdavian, *Carbohydr. Polym.*, 2018, **200**, 583–594.
- 27 A. Abdollahi, J. K. Rad and A. R. Mahdavian, *Carbohydr. Polym.*, 2016, **150**, 131–138.
- 28 M. Q. Zhu, G. F. Zhang, Z. Hu, M. P. Aldred, C. Li, W. L. Gong, T. Chen, Z. L. Huang and S. Liu, *Macromolecules*, 2014, **47**, 1543–1552.
- 29 E. Fleige, M. A. Quadir and R. Haag, *Adv. Drug Delivery Rev.*, 2012, **64**, 866–884.
- 30 S. Swaminathan, J. Garcia-Amorós, A. Fraix, N. Kandoth, S. Sortino and F. M. Raymo, *Chem. Soc. Rev.*, 2014, **43**, 4167–4178.
- 31 M. Motornov, Y. Roiter, I. Tokarev and S. Minko, *Prog. Polym. Sci.*, 2010, **35**, 174–211.
- 32 J. E. Stumpel, D. J. Broer and A. P. H. J. Schenning, *Chem. Commun.*, 2014, **50**, 15839–15848.
- 33 S. Wang, P. Huang and X. Chen, *ACS Nano*, 2016, **10**, 2991–2994.
- 34 H. Che and J. C. M. Van Hest, *J. Mater. Chem. B*, 2016, **4**, 4632–4647.
- 35 A. P. Blum, J. K. Kammeyer, A. M. Rush, C. E. Callmann, M. E. Hahn and N. C. Gianneschi, *J. Am. Chem. Soc.*, 2015, **137**, 2140–2154.
- 36 C. W. Huang, W. Y. Ji and S. W. Kuo, *Polym. Chem.*, 2018, **9**, 2813–2820.
- 37 S. Hajebi, A. Abdollahi, H. Roghani-Mamaqani and M. Salami-Kalajahi, *Polymer*, 2019, **180**, 121716.
- 38 B. Razavi, A. Abdollahi, H. Roghani-Mamaqani and M. Salami-Kalajahi, *Mater. Sci. Eng., C*, 2020, **109**, 110524.
- 39 S. Hajebi, A. Abdollahi, H. Roghani-Mamaqani and M. Salami-Kalajahi, *Langmuir*, 2020, **36**(10), 2683–2694.
- 40 Z. Abousalman-Rezvani, P. Eskandari, H. Roghani-Mamaqani and M. Salami-Kalajahi, *Carbohydr. Polym.*, 2019, **225**, 115247.
- 41 A. Mousavi, H. Roghani-Mamaqani, M. Salami-Kalajahi, S. Shahi and A. Abdollahi, *EXPRESS Polym. Lett.*, 2018, **12**, 187–202.
- 42 A. Abdollahi, Z. Alinejad and A. R. Mahdavian, *J. Mater. Chem. C*, 2017, **5**, 6588–6600.
- 43 B. Razavi, A. Abdollahi, H. Roghani-Mamaqani and M. Salami-Kalajahi, *Polymer*, 2020, **187**, 122046.
- 44 J. Ter Schiphorst, J. Saez, D. Diamond, F. Benito-Lopez and A. P. H. J. Schenning, *Lab Chip*, 2018, **18**, 699–709.
- 45 Y. Zhao, *Macromolecules*, 2012, **45**, 3647–3657.
- 46 F. D. Jochum and P. Theato, *Chem. Soc. Rev.*, 2013, **42**, 7468–7483.
- 47 Y. Fu, H.-H. Han, J. Zhang, X.-P. He, B. L. Feringa and H. Tian, *J. Am. Chem. Soc.*, 2018, **140**, 8671–8674.
- 48 J. Zhang, Y. Fu, H.-H. Han, Y. Zang, J. Li, X.-P. He, B. L. Feringa and H. Tian, *Nat. Commun.*, 2017, **8**, 987.
- 49 R. Heiligman-Rim, Y. Hirshberg and E. Fischer, *J. Chem. Soc.*, 1961, 156.
- 50 M. E. Genovese, E. Colusso, M. Colombo, A. Martucci, A. Athanassiou and D. Fragouli, *J. Mater. Chem. A*, 2017, **5**, 339–348.
- 51 M. Qin, Y. Huang, F. Li and Y. Song, *J. Mater. Chem. C*, 2015, **3**, 9265–9275.
- 52 M. Li, Q. Zhang, Y. N. Zhou and S. Zhu, *Prog. Polym. Sci.*, 2018, **79**, 26–39.

- 53 K. Wagner, R. Byrne, M. Zanoni, S. Gambhir, L. Dennany, R. Breukers, M. Higgins, P. Wagner, D. Diamond, G. G. Wallace and D. L. Officer, *J. Am. Chem. Soc.*, 2011, **133**, 5453–5462.
- 54 A. Abdollahi, A. Herizchi, H. Roghani-Mamaqani and H. Alidaei-Sharif, *Carbohydr. Polym.*, 2020, **230**, 115603.
- 55 M. Q. Zhu, L. Zhu, J. J. Han, W. Wu, J. K. Hurst and A. D. Q. Li, *J. Am. Chem. Soc.*, 2006, **128**, 4303–4309.
- 56 Y. M. Wang, X. T. Tian, H. Zhang, Z. R. Yang and X. B. Yin, *ACS Appl. Mater. Interfaces*, 2018, **10**, 22445–22452.
- 57 Q. Qi, C. Li, X. Liu, S. Jiang, Z. Xu, R. Lee, M. Zhu, B. Xu and W. Tian, *J. Am. Chem. Soc.*, 2017, **139**, 16036–16039.
- 58 F. Li, X. Wang, Z. Xia, C. Pan and Q. Liu, *Adv. Funct. Mater.*, 2017, **27**, 1700051.
- 59 J. Fölling, S. Polyakova, V. Belov, A. Van Blaaderen, M. L. Bossi and S. W. Hell, *Small*, 2008, **4**, 134–142.
- 60 X. Tian, B. Wang, J. Li, J. Zeng and K. Chen, *Carbohydr. Polym.*, 2017, **157**, 704–710.
- 61 S. Kalytchuk, Y. Wang, K. Poláková and R. Zbořil, *ACS Appl. Mater. Interfaces*, 2018, **10**, 29902–29908.
- 62 F. M. Raymo, S. Giordani, A. J. P. White and D. J. Williams, *J. Org. Chem.*, 2003, **68**, 4158–4169.
- 63 A. Saad, O. Oms, A. Dolbecq, C. Menet, R. Dessapt, H. Serier-Braut, E. Allard, K. Baczko and P. Mialane, *Chem. Commun.*, 2015, **51**, 16088–16091.
- 64 Z. Wu, K. Pan, S. Mo, B. Wang, X. Zhao and M. Yin, *ACS Appl. Mater. Interfaces*, 2018, **10**, 30879–30886.
- 65 W. K. Tsai, Y. S. Lai, P. J. Tseng, C. H. Liao and Y. H. Chan, *ACS Appl. Mater. Interfaces*, 2017, **9**, 30918–30924.
- 66 W. Huang, M. Xu, J. Liu, J. Wang, Y. Zhu, J. Liu, H. Rong and J. Zhang, *Adv. Funct. Mater.*, 2019, **29**, 1808762.